

Electronic Supplementary Material for “Stress-induced surface instabilities and defects on thin films sputter deposited on compliant substrates”

Timothy Ibru,^a, Kyriaki Kalaitzidou^{a,b}, J. Kevin Baldwin^c and Antonia Antoniou^a

a. G.W. Woodruff School of Mechanical Engineering, Georgia Institute of Technology, Atlanta GA 30332.

b. School of Materials Science and Engineering, Georgia Institute of Technology, Atlanta GA 30332

c Center for Integrated Nanotechnologies (CINT), Los Alamos National Laboratory, Los Alamos, NM, 87545

Calibration of PDMS spin speed versus thickness

In order to confirm relationship between spin speed and the PDMS thickness, a simple calibration procedure was conducted. All PDMS samples were prepared on a glass slide. Steps were created on these glass slides, cut out with a blade. A profilometer was then passed over the steps and the change in path due to the step was measured. Cuts were made at different positions to account for possible variations in thickness. These variations were accounted for in the standard deviations of the charts. The schematic of the profilometer location scans is shown on Fig. SM1(a) and Fig. SM1(b) shows the dependence of the PDMS thickness on the spin speed

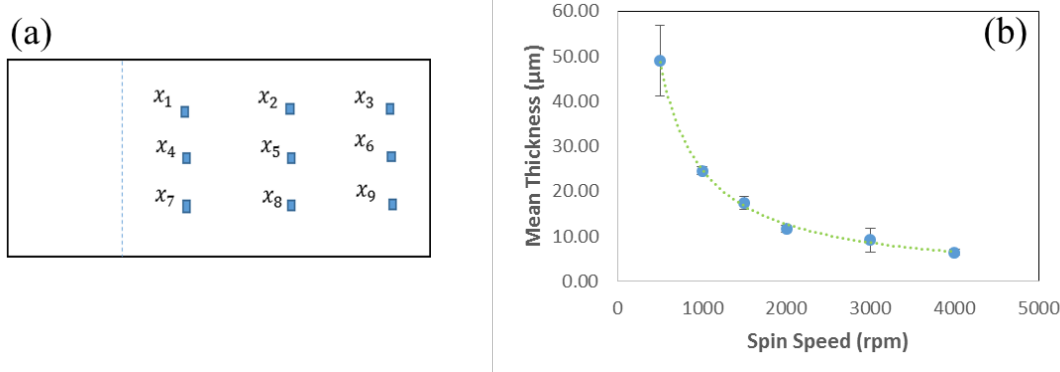


Figure SM1: (a) Schematic of the profilometer measurement locations (b) Average Measured Thickness vs. Spin Speed

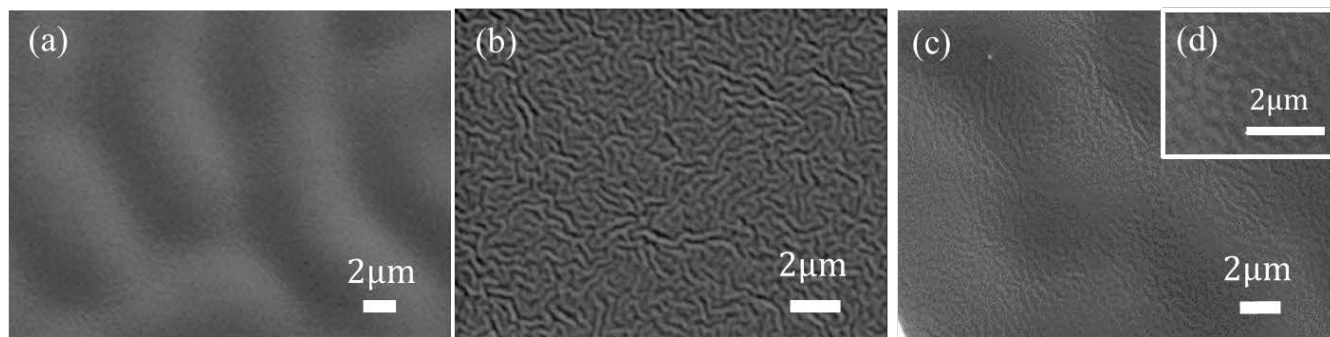


Figure SM2: Plan view SEM images of the bilayer surface after deposition of the coating. (a) 25/110/UVPDMS/Au-Ag; (b) 6/70PDMS/Au₂₀Si₈₀. (c) and (d) show 9/150PDMS/Au₂₀Si₈₀ at two different magnifications so that nested wrinkles become clearly visible.

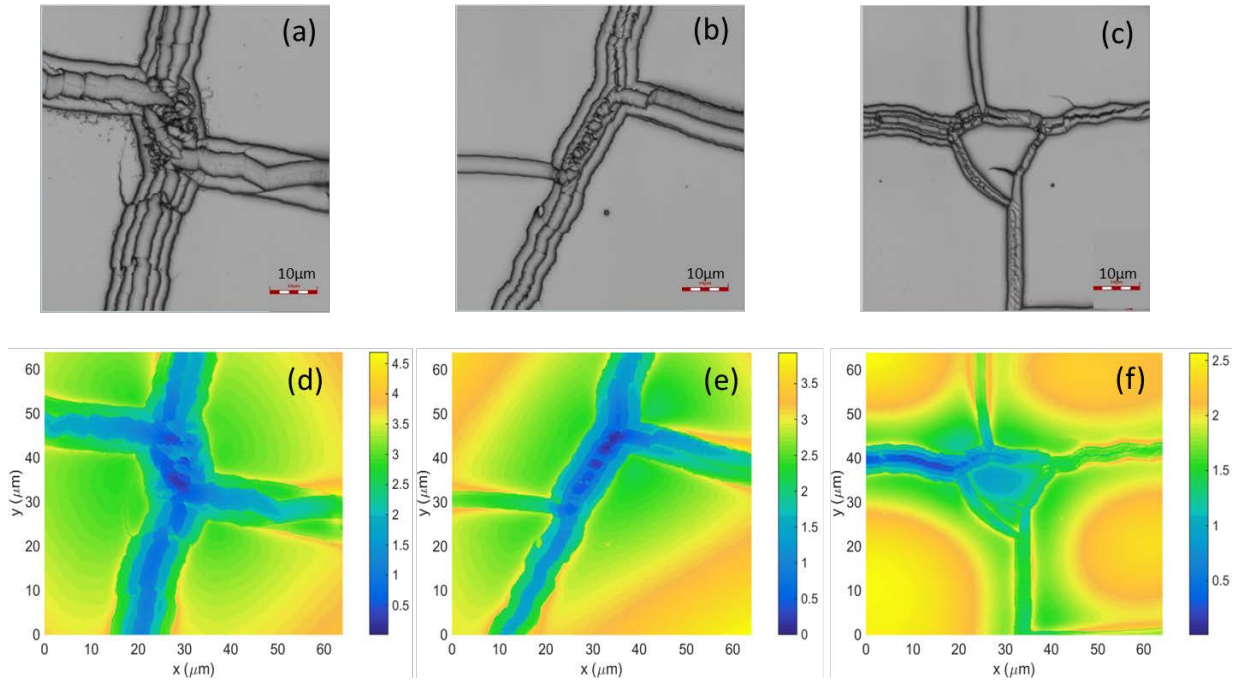


Figure SM3: Confocal (a-c) planar and (d-e) depth profile images of UV treated PDMS samples.

Note the large opening depth of the samples. Samples correspond to (a),(d) $h_s = 50\mu\text{m}$, (b),(e) $h_s = 27\mu\text{m}$ and (c),(f) $h_s = 6\mu\text{m}$ thickness respectively. The crack depth (a) and crack opening displacement for the UV treated samples were calculated from these datasets.

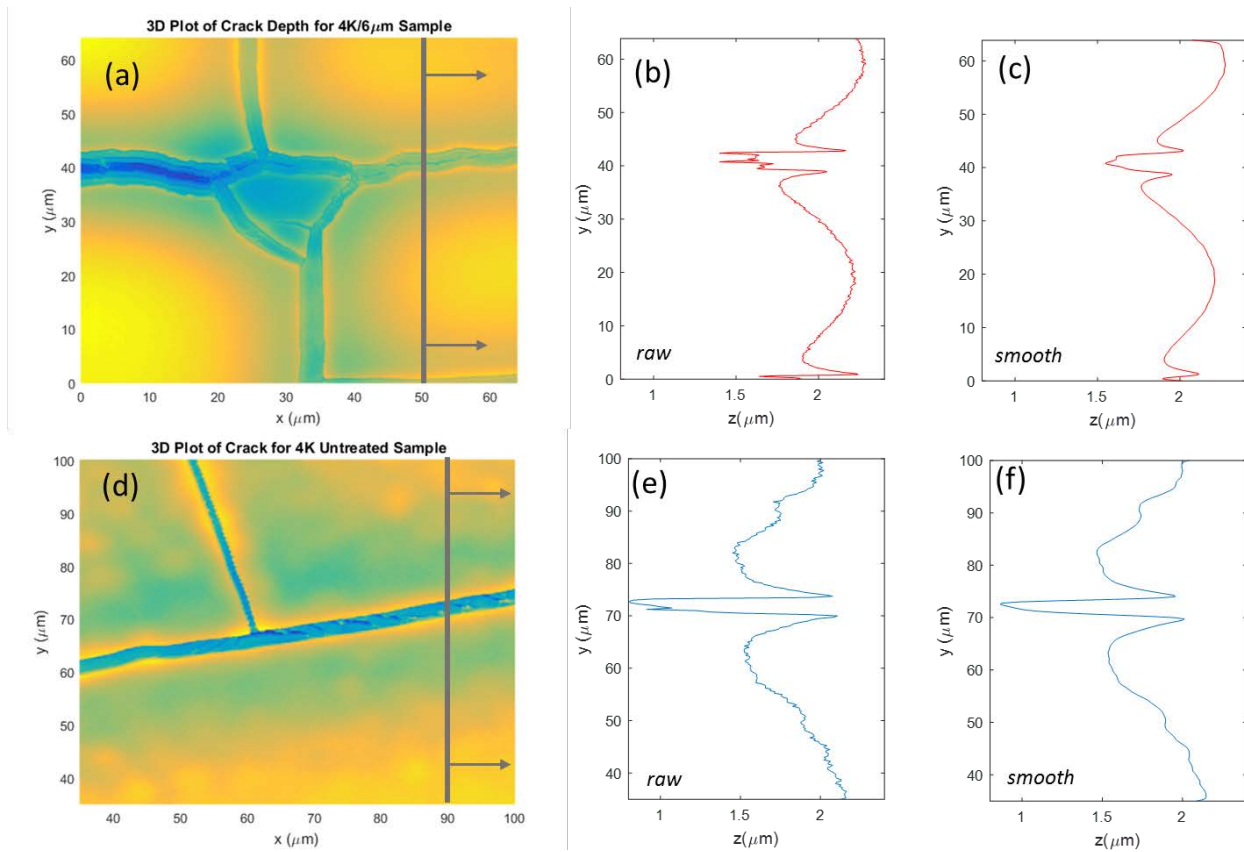


Figure SM4: Confocal depth profile images of Au-Si deposited on (a-c) UV treated and (d-e) not UV treated PDMS samples of the same overall thickness. The 1D plots of the surface profile before (b),(e) and after (c), (f) filtering of the data is shown. There is a remnant on the untreated UV sample coating which on close inspection from the SEM images is more of a

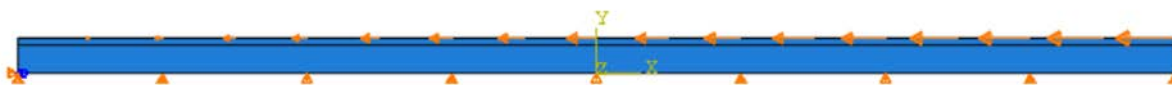


Figure SM5. The boundary conditions used for the numerical model. Only the bottom side of the PDMS substrate is constrained. Close to the bilayer interface, a continually increasing compressive displacement is applied (Case 1 or Case 2).

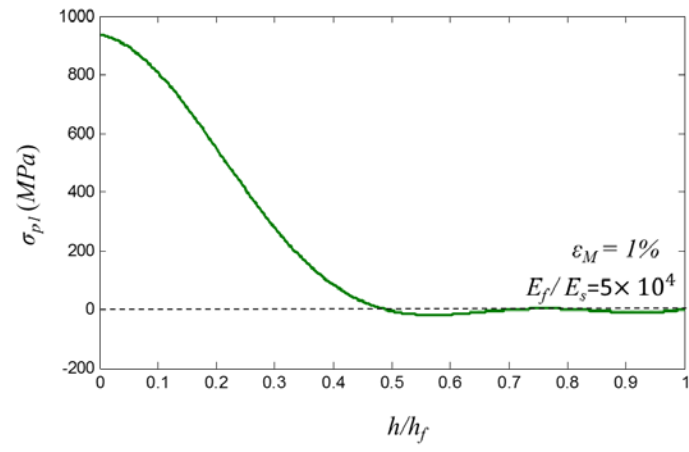


Figure SM6. Principal stress profile through the film thickness for Case 1.

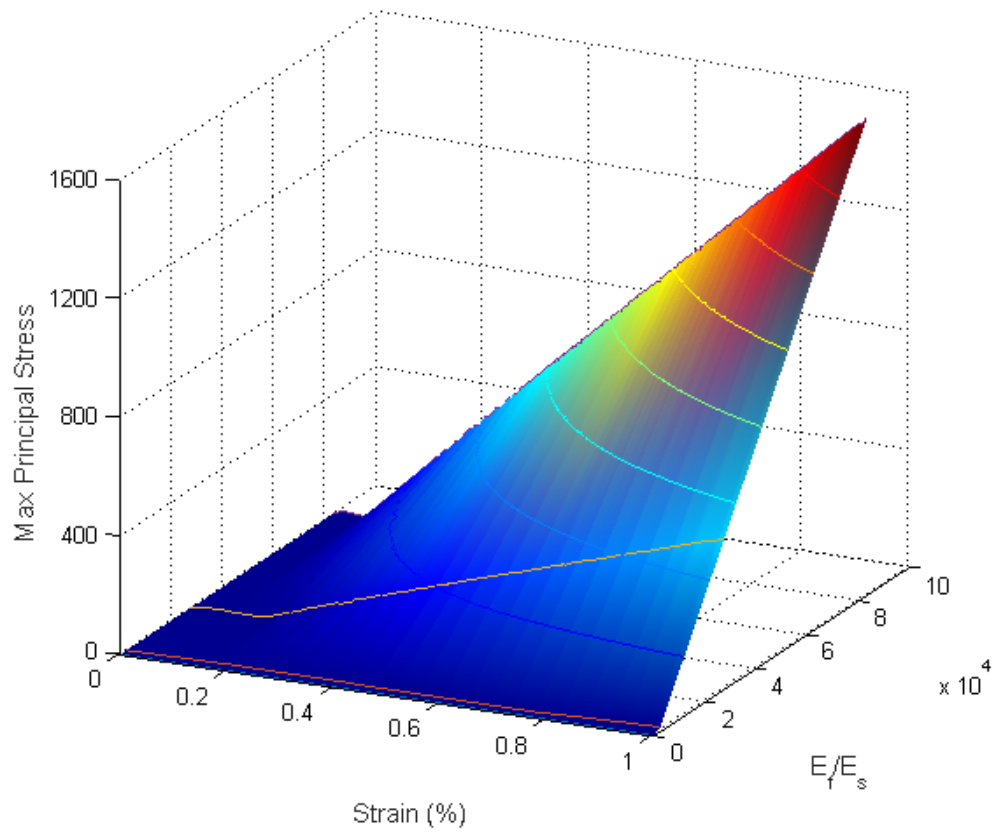


Figure SM7. Finite Element Predictions for the maximum tensile principal stress (MPa) at the peak of wrinkles as a function of applied mismatch strain and film to substrate modulus ratio. For this case, $t_f=70\text{nm}$.

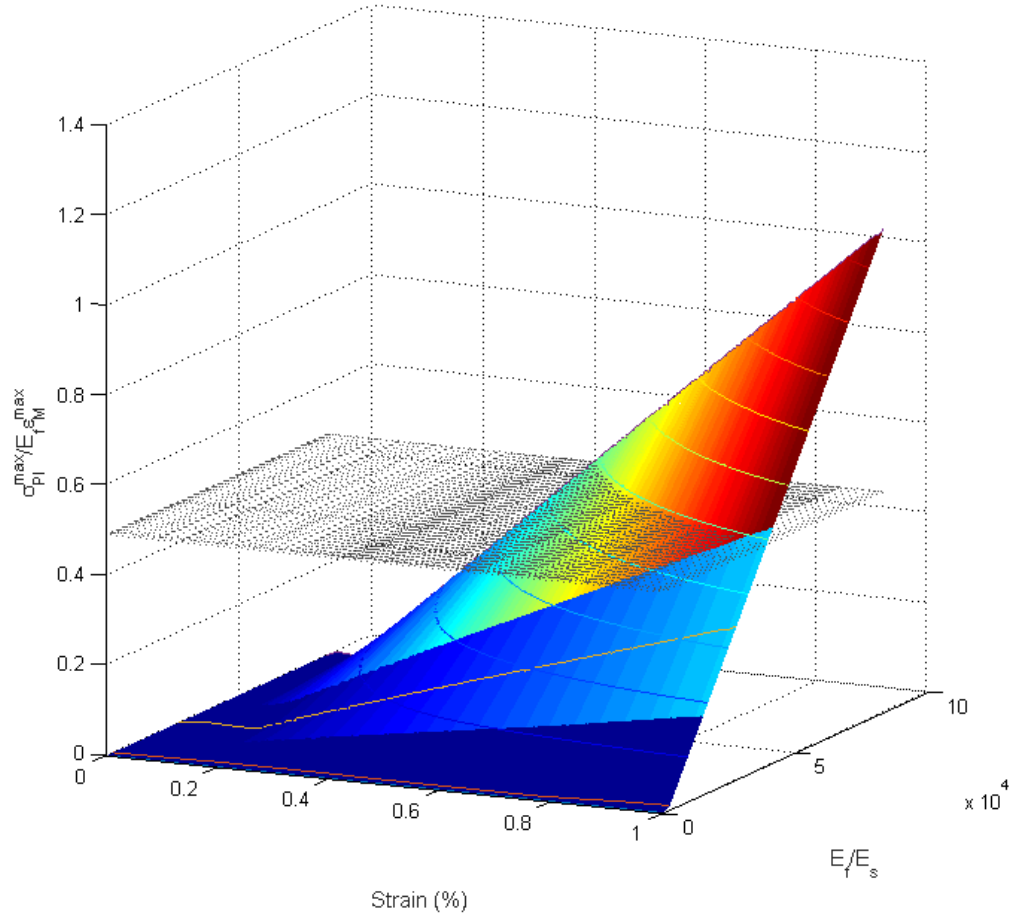


Figure SM8. Finite Element Predictions for the maximum tensile principal stress at the peak of wrinkles normalized with the film modulus and maximum applied compressive strain at the interface. The normalized peak stress is shown as a function of applied mismatch strain and film to substrate modulus ratio. The grey horizontal line corresponds to a value of $K_{IC}/Z=0.01$. For this scenario, $t_f=70\text{nm}$.